

Comparative analysis of Airborne and Terrestrial survey of Odeda Lithology, Ogun State, Nigeria, using Radiometric approach

*Ogunsanwo, F.O., Ayanda, J.D., Okusanya, A.A., Adelaja, A.D., Falayi, E.O. & Oyebanjo, O.A.
Physics Department, Tai Solarin University of Education, Ijagun, Ogun State, Nigeria
Corresponding Author Email: godif07@yahoo.com*

ABSTRACT

Airborne radiometric survey (ARS) is now been used to compliment the terrestrial radiometric survey (TRS) due to the wider coverage capability with highly sensitive automated radiometric survey meter. In this study, ARS and TRS were carried out to examine the radiometric behaviour of weathered basement in Ogun state for uranium, thorium, potassium alongside their total count. ARS radiometric data was collected from the radiometric department of Nigerian Geological Survey Agency, Abuja, Nigeria, in line with the sampling point coordinate of TRS. The TRS was done by collecting soil samples randomly across the weathered basement area and transferred to Institute of radiation protection center laboratory, University of Ibadan, for radiometric analysis. For comparison, the two surveys were subjected to regression analysis, normalisation test, homogeneity test and geochemical superposition. The regression analysis was used to generate the empirical model connecting the two surveys for each radiometric components. The degree of fitness, coefficient of correlation and spatial distribution of the two surveys were as well computed and constructed. The result obtained showed more elevated concentrations of uranium and thorium in ARS compared to TRS. The total count accounted for thorium as its major prevalence radioelement constituent. The spatial distribution of uranium showed a reflection of high similarity index in both the ARS and TRS with elevated response around pegmatite unit. The homogeneity test revealed high coefficient of variation values ($CV > 50\%$) in the radioelements which implies that the radioelements are not from a single sources. The regression models developed for ARS and TRS accounted for good correlation coefficient of 81%, 71%, 76% and 71% for uranium, thorium, potassium and total count, respectively. This study has, therefore, proven the two radiometric survey methods to be comparable and efficient in delineating the radiometric anomaly associated with the study area.

Keywords: radiometric; terrestrial; weathered; models; spatial

INTRODUCTION

Radiometric method has been found to be widely used in investigating and providing detailed information about the distributions and concentrations of the primordial radionuclides (eU, eTh, K) in any specific areas. The naturally occurring radionuclides are present in the rock, soil and are easily transported into the environment through plants and water (Eisenbud and Gesell, 1997; Murugesan *et al.*, 2011).

The application of uranium, thorium and potassium in the field of science and technology cannot be over-emphasize. Their contribution is greatly felt in agriculture for making fertilizer, nuclear plant where uranium and thorium serves as the nuclear fuel (Ye *et al.*, 2019; Steiner *et al.*, 2020; Haneklaus, 2021; Sun *et al.*, 2022). Contrarily, it bring about adverse effect on human when excessively exposed to them such as lung and cancer disease. Therefore deposition level of the radioelements concentration needs to be assessed from time to time in order to provide the quality management of the environment.

Gamma ray spectrometric methods have been widely used in measurements of radioactive minerals in soils and basement rocks (Abuelnaga and Al-Garni, 2015). The radioactive distribution is not uniform and depends on lithology and extent of mineralization of the formation rocks in a given area (Faure, 1986; Menager *et al.*, 1993; Tzortzis and Tsertos, 2004). Radiometric response varies from geology to geology and climate to climate. Mostly, basement terrain used to accounts for elevated radiometric

response while sedimentary formation are associated with low radiometric signature. The sedimentary area characterised by shale and sandstone have been reported by UNSCEAR (1993) and McCay *et al.* (2014) to have relatively high radiometric value.

The three radioelements are associated with long half life and hardly disintegrate but their emission and distribution can be altered by natural phenomenon and anthropogenic activities (IAEA, 2003). Several factors such as topography, vegetation cover, temperature, soil moisture and precipitation can alter their distribution (Ogunsanwo *et al.*, 2019).

The use of airborne radiometric survey is now commonly used, although it is very expensive, but it covers a large land mass within short time compared to ground radiometric survey. The recent work on radiometric response of different geological terrain using the airborne and ground radiometric survey have been reported in different literatures such as Polito *et al.* (2011), Ramadass *et al.* (2015), Carvalho *et al.* (2011), Olorunsola and Aigbogun (2017), Abbady and Al-Ghamdi (2018), Hasterok *et al.* (2018), Adagunodo *et al.* (2019), Veikkolainen and Kukkonen (2019), Ogunsanwo *et al.* (2021) and many others, in delineating possible mineral deposit, geothermal explorations, identification of faults and fractures, estimating the radiometric flux behaviour and anomalous responses across different bedrock stratigraphy.

The lithology of the study area is characterised by weathered basement, therefore the response to radiometric response need to be examined and provide baseline information for other formations with similar bedrock composition. The main objectives of this study are to analyze the radioactive content qualitatively, establish empirical relation between ground and airborne survey, and to determine the radiometric anomaly in relation to the bedrock composition.

MATERIALS AND METHODS

Location and Geological Setting of the study Area

Odeda, the study area, falls between longitudes $3^{\circ}26'76''$ and $3^{\circ}47'28''$ and latitudes $7^{\circ}29'88''$ and $7^{\circ}05'54''$ in Ogun State, Nigeria. It has a land mass area of $1,560 \text{ km}^2$ and falls within the tropical rainforest zone. The temperature ranges between 28°C to 34°C , while the mean annual rainfall experienced is about 1800 mm yr^{-1} . The study area falls on the tropical rainforest climatic condition with two distinct seasons; namely dry and monsoon (heavy down pour). The study area is notable with quarries where blasting of rock is the major industrial activities aside from farming.

The study area is weathered basement complex terrain which harbors varieties of outcrops. The geological composition of the study area mainly consists of migmatite, pegmatite, coarse-porphyrific biotite and biotite, muscovite granite, Abeokuta formation (shale and sandstone) and pyroxene diorite (Figure 1). The older granites are late Precambrian to early Palaeozoic and are of magmatic origin (Rahaman, 1976; Omatsola and Adegoke, 1981; Badmus *et al.*, 2010). The identified lithogenic rock compositions in the study area have great tendency to be accompanied by radioelement emission when blasted. The blasting activities bring about the chemical, biological and mechanical decomposition of rocks. These decompositions may greatly affect the tectonic structure of the geological plate resulting into weathering and landslide movements (Peng *et al.*, 2019; Yu *et al.*, 2021; Fu *et al.*, 2022). Studies of weathered tropical soils have revealed that the geology of bedrock has a significant influence on soil distribution and nature (Talabi, 2015).

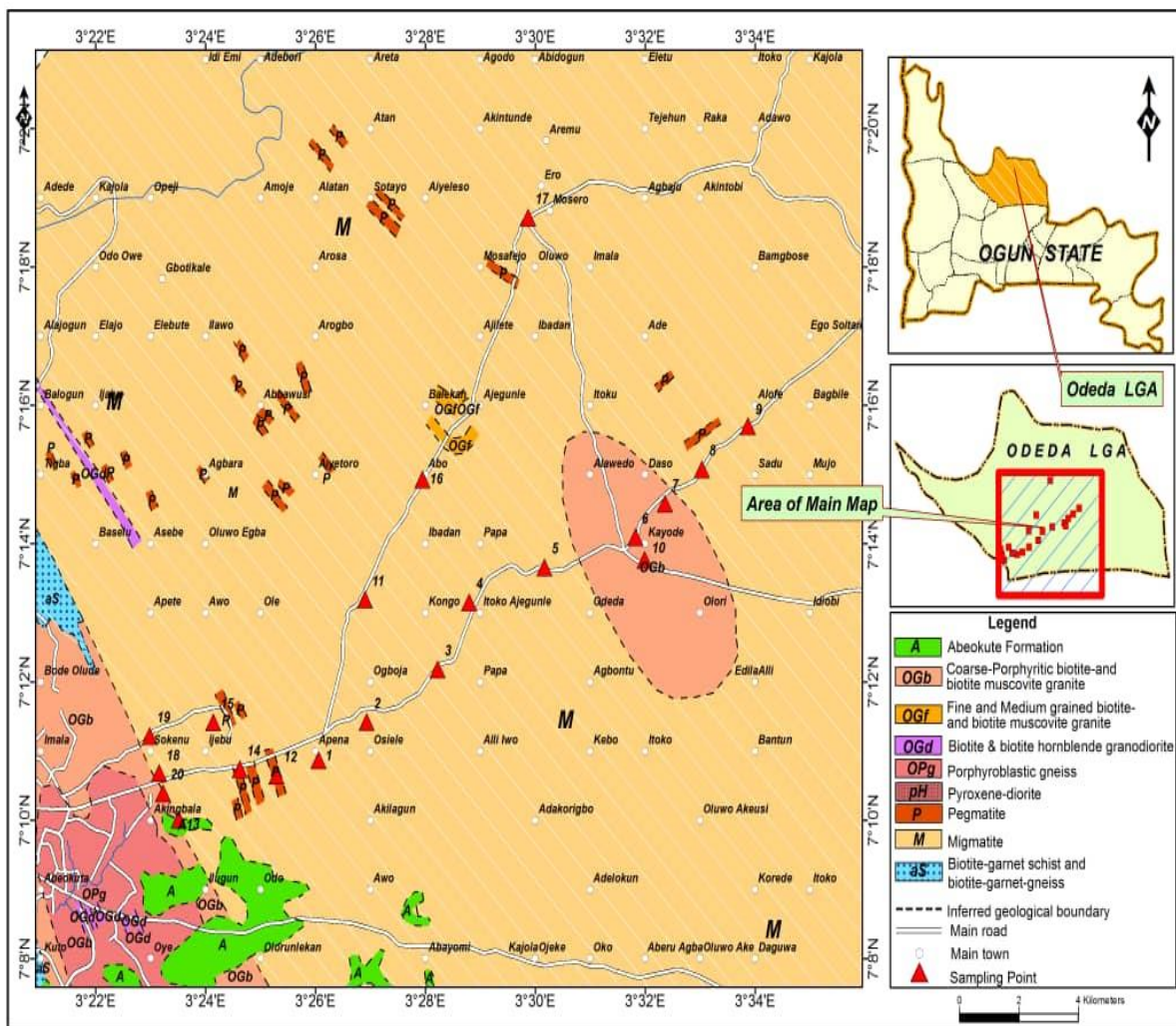


Figure 1: Geological map showing the sampling points

Radiometric data acquisition

Airborne data acquisition

In 2009, Nigeria Geological Survey Agency (NGSA) carried out an airborne survey over the study area with a gamma spectrometer at a flight line separation of 200–500m flown at a planned terrain clearance of 120m. With the aid of a highly sensitivity 256-channel airborne gamma spectrometer (AGRS) system comprising of 321 of downward-looking NaI (TI) (Sodium Iodide crystals treated with thallium) detector and 81 of upward-looking detector the radiometric data were acquired. Uranium (^{238}U) is estimated through the radon daughter ^{214}Bi in its decay chain, while thorium (^{232}Th) is estimated through ^{208}Tl in its decay chain. Potassium is measured directly at 1.461 MeV. The Potassium value was recorded directly in percent (%) while the equivalent value of thorium, eTh, and Uranium, eU, were obtained in part per million (ppm) (NGSA, 2019; Ogunsanwo, 2019).

Ground data acquisition

A ground survey was carried out around Odeda, the weathered area, where soil samples were taken from 20 different locations characterised by diverse bedrock composition (Figure 1). The sampling points were picked in such a way that it matched with that of the airborne data set coordinates (Table

1). The soil samples were collected randomly from different locations across the study area using a hand auger at depth of about 7 cm. It is ensured that the collected soil samples were perfectly sieved, sun dried to about 100°C and then left for about 28 days in order to attain secular equilibrium before they were taken to the laboratory for gamma spectrometric analysis. Radioactivity measurement was carried out at the Radiation Laboratory, Department of Physics, University of Ibadan, Ibadan using the NaI(Tl) detector coupled to the digibase multichannel analyser. The system calibration was performed using International Atomic Energy Agency (IAEA) reference materials RGK-1, RGU-1 and RGTh-1 for K, U and Th activity measurements respectively. The procedure for calibration and measurements were adopted from Grasty *et al.* (1991). The ground concentrations for K, eTh and eU were recorded in Becquerel per Kilogram (Bqkg⁻¹).

Table 1: The sample location coordinates and its bedrock characterization

S/N	Location	Sample Code	Latitude	Longitude	Bedrock Composition
1	Fatola Estate Camp	OD1	7.18112	3.43428	Migmatite
2	Ire Akari Osiele	OD2	7.19030	3.44890	Migmatite
3	Arugbokosun	OD3	7.20304	3.47040	Migmatite
4	Aderupoko	OD4	7.21918	3.47996	Migmatite
5	Rogan Church	OD5	7.22763	3.30283	Migmatite
6	Odeda L.G.A Sec.	OD6	7.23485	3.53049	Coarse-porphyratic biotite and muscovite
7	Paragon/ Ajegunle	OD7	7.24299	3.53936	Coarse-porphyratic biotite and muscovite
8	Akankan Town	OD8	7.25124	3.55062	Migmatite
9	Saadu Village	OD9	7.26161	3.56460	Migmatite
10	Railway Station Odeda	OD10	7.22943	3.53321	Coarse-porphyratic biotite and muscovite
11	Funaab Zoo	OD11	7.12986	3.44834	Migmatite
12	Emere Village	OD12	7.17741	3.42153	Pegmatite
13	Arokoje	OD13	7.16677	3.39193	Sandstone
14	Aregbe Rosiji Street	OD14	7.17894	3.41039	Pegmatite
15	Ifesowapo Aponte	OD15	7.19023	3.40232	Migmatite
16	Alabata Road	OD16	7.24877	3.46581	Migmatite
17	Alabata Market	OD17	7.31196	3.49789	Migmatite
18	Asero Mountain Of Fire	OD18	7.17799	3.38591	Pegmatite
19	Ijemo	OD19	7.18697	3.38304	Migmatite
20	Back Of Stadium	OD20	7.17317	3.38715	Coarse-porphyratic biotite and muscovite

RADIOMETRIC DATA ANALYSIS

Qualitative analysis of the data was carried out such that it provides information directly interpretable in terms of surface geology.

Conversion of radiometric data

The ground concentration was converted from $Bqkg^{-1}$ to ppm and % using conversion factor as given by Polish Central Laboratory for Radiological Protection (Malczewski *et al.* 2004) as shown in Equations 1 – 3 for uranium in ppm, thorium in ppm and potassium in %, respectively.

$$C_U(\text{ppm}) = C_U(Bqkg^{-1}) \times 0.08045 \quad (1)$$

$$C_{Th}(\text{ppm}) = C_{Th}(Bqkg^{-1}) \times 0.24331 \quad (2)$$

$$C_k(\%) = C_k(Bqkg^{-1}) \times 0.003296 \quad (3)$$

where C_U , C_{Th} and C_k are the concentrations of ^{238}U , ^{232}Th and ^{40}K , respectively.

Total count estimation

This comprises of the net radioactivity due to the three radioelements, U, Th and K in proportion as given by Ashwal *et al.* (1987), Singh and Vallinayagam (2004) in equation (4)

$$TC(Ur) = C_U(\text{ppm}) + 2C_{Th}(\text{ppm}) + 0.5C_K(\%) \quad (4)$$

Linear regression model estimation

In this study, linear regression approach was used to establish a relationship between the ground and airborne radiometric survey, and vice versa for the study area. The airborne to ground radiometric linear models are deduced from relation proposed in Equation (5 – 8):

$$U_{ARS} = pU_{GRS} + q \quad (5)$$

$$Th_{ARS} = pTh_{TRS} + q \quad (6)$$

$$K_{ARS} = pK_{TRS} + q \quad (7)$$

$$TC_{ARS} = pTC_{TRS} + q \quad (8)$$

The ground to airborne radiometric linear models are estimated from the proposed relation given by Equations (9- 12):

$$U_{TRS} = pU_{ARS} + q \quad (9)$$

$$Th_{TRS} = pTh_{ARS} + q \quad (10)$$

$$K_{TRS} = pK_{ARS} + q \quad (11)$$

$$TC_{TRS} = pTC_{GRS} + q \quad (12)$$

where,

U_{ARS} , Th_{ARS} and K_{ARS} are the airborne radiometric concentrations data set for uranium, thorium and potassium respectively.

U_{TRS} , Th_{TRS} and K_{TRS} are the terrestrial (ground) radiometric concentrations data set for uranium, thorium and potassium respectively.

p and q are correctional constant to be determined

Coefficient of variation

The coefficient of variation (CV) indicates the degree of variability in the concentration of the two surveys. If coefficient of variation is low (i.e. $CV \leq 50\%$), it implies that the variability is low (homogeneous), while coefficient of variation value above 50% is considered as high variability (heterogeneous) (Karim *et al.*, 2015). It is always express in percentage with different range specifying the degree of homogeneity. It is therefore formulated as given in equation (13):

$$CV(\%) = \frac{S}{X} \times 100 \quad (13)$$

where

S is the standard deviation of the data set

X is the mean of the data set.

RESULTS AND DISCUSSION

Radiometric response to lithology

The response of radioelements and their total count from the two survey are as presented in Figures 2 (a – d). Uranium was found to have elevated response at OD7 and OD18 while the lower concentrations are found associated with OD2, OD5, OD8, OD11, OD15 and OD17 both for TRS and ARS (Figure 2a). the capacity of enhancing the uranium concentration (Wilton and Cunningham-Dunlop, 2006). Pegmatite according to NCRP (1984) has been identified as one of host rock of uranium in granitic rocks. The elevated response are due to the lithogenic rock characterization due to pegmatite and muscovite which have The units with low uranium concentration consists of migmatite as dominant rocks. Migmatite is a metamorphosize igneous rock, which during the rock decomposition allows depletion of uranium concentration. This may be the consequence of either the underlying or overlying bedrock units which has been eroded by weathering or other geomorphic processes.

Thorium showcased similar elevated radiometric signature at OD3, OD7, OD12 and OD19 in both TRS and ARS (Figure 2b). Thorium unlike uranium is an immobile element and have the tendency of not being totally eroded by any geological or geomorphic processes, hence resulting in its concentration enhancement at those lithological units. TRS accounted for the highest thorium response at OD10 which does not correspond with ARS. The slight disparity may be due to soil moisture and precipitation which have the capacity of elevating the ground thorium response. The lower concentration responses were observed at OD4, OD6, OD8, OD9, OD11 and OD17 (Figure 2b). The composition of the six identified low thorium response units are migmatite and biotite. The formation of these rocks may attenuate thorium radioactive concentrations aside from being eroded.

Potassium response is most elevated at OD2 and OD4, but slightly increases at units OD8, OD10 and OD19 both in TRS and ARS. OD13, OD16, OD18, and OD20 experienced potassium increases only in ARS but tend to attenuate in TRS. OD1, OD5, OD7, OD9, OD12, OD15 and OD17 (Figure 2c) accounted for low potassium concentration response both at TRS and ARS. The result showed that potassium response is attenuated in migmatite rock composition. It was observed that potassium has an inverse response with uranium and thorium at OD7 and OD12. This may be due to the fact that pegmatite and muscovite which have strong affinity for uranium and thorium quickly leached away potassium through weathering and biodegradation.

The total count comprises of summation of uranium, thorium and potassium concentrations in proportion. The result obtained points to the fact that their is reflection of high similarity of thorium signature in total count (Figure 2d). This implies larger percentage of thorium (about 67.3 %) are found in the total count compared to the uranium and potassium.

Generally, the ARS survey accounted for higher quantity of uranium and thorium concentration compared to TRS but their signature similarity index is relatively high. Potassium on the other has experienced higher TRS response compared to ARS. Potassium is very reactive alkaline metal which are more available and detectable at low altitude while the ARS response to potassium may be hindered by natural geomorphic formation process

Radiometric Spatial distribution

In this study, the spatial distribution of radioelements and their total count were assessed using contour map. The contour maps were constructed with the help of geosoft (Oasis montaj) software. The contour plot in Universal Transverse Mercator (UTM) helps in the delineation of surface distribution pattern of the radioelement over the study area (Ogunsanwo, 2019). The spatial distribution of TRS and ARS for potassium, thorium, uranium and total count were presented in contours form (Figures 3 – 6) in order to delineate the region with anomalous radiometric response with lithology. The concentration prevalence level were classified into three distinct group; the low response is assigned with light –deep blue, the moderate response is denoted with greenish-yellow colour while the intense/high prevalence are represented with reddish-pink colour.

The potassium spatial distribution for ARS and TRS are illustrated by Figures 3(a and b), respectively. The potassium contour map with gridded concentration was found ranging from -1.325 to 0.488 % as obtained for TRS and -0.610 to 1.664 % for ARS. In ARS (fig 3a), the three prevalence levels are identified such that the low response are observed in the upper NE corner and NW part of the study area. The moderate prevalence response formed a boundary at the center demarcating the high and low response. The high potassium response is found at a spot in the extreme northern section and extensively in the eastern and SW part of the study area. Comparably, the TRS (Fig 3b) showcase similar occurrence of low and moderate prevalence levels, but the high prevalence are found appear stronger in the SE corner and are continuous unlike ARS where the high prevalence are disjointed. High similarity with little disparity are found in the constructed potassium prevalence distribution for both ARS and TRS.

The distribution of thorium was presented by Figures (4a and b) for ARS and TRS respectively. Thorium contour maps show that the concentrations range from -3.057 to 13.386 ppm and 1.852 to v

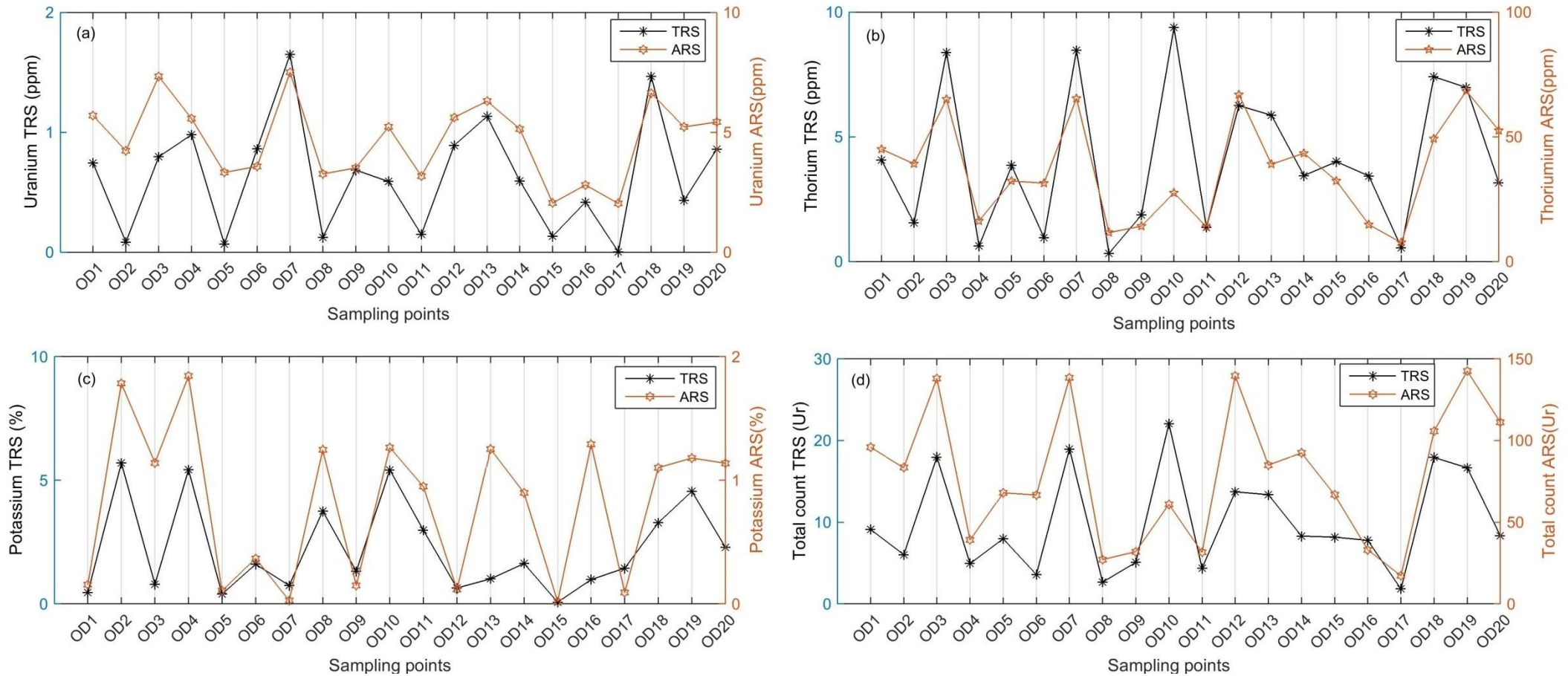
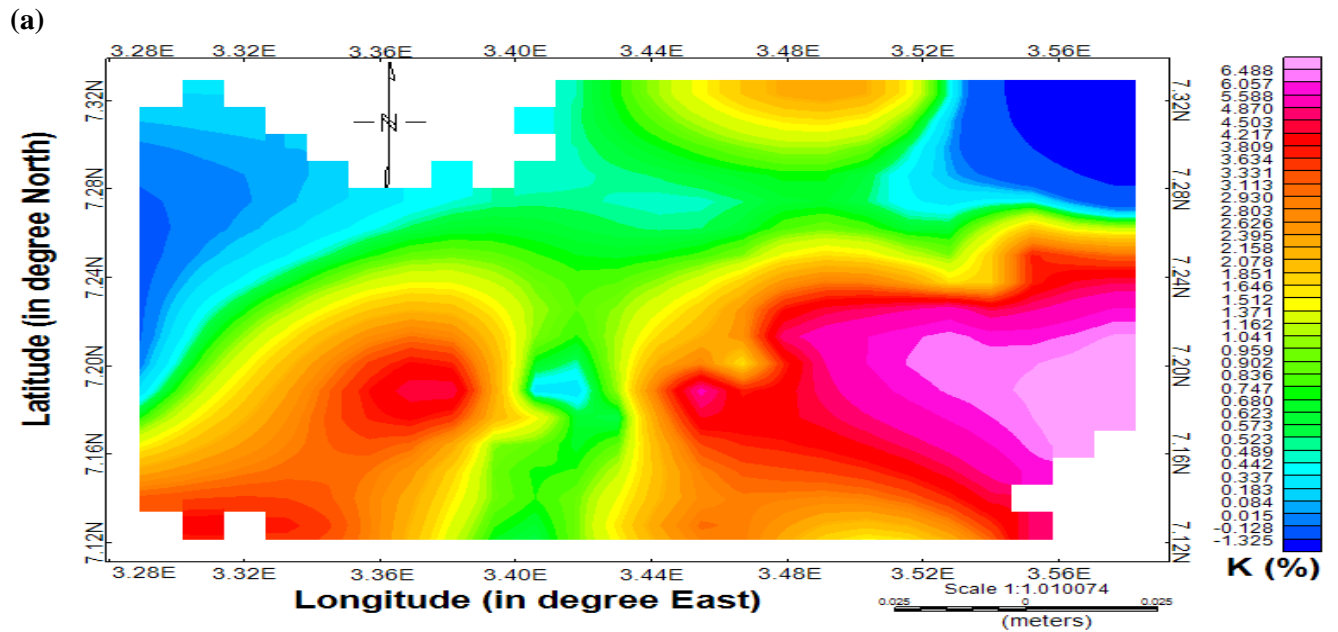


Figure 2: ARS and TRS radiometric variation response for (a) Uranium (b) Thorium (c) Potassium (d) Total count across the lithology

The contour maps for uranium varied from 1.317 to 7.522 ppm for TRS and -0.162 to 1.637 ppm for ARS. The uranium anomalous response was found it have its low concentration at three different spots in ARS (Fig. 5a), in the NW, central and upper Northern section while in TRS the low prevalence response appear like a large oval in the upper northern part migrating centrally. This implies that the isolated central and upper Northern section low prevalence in ARS are joined in the TRS. (Fig. 5b). The intense prevalence response appear in a continuous form in the southern (SW, SS and SE) section of the study area. High similarity index occur in the intense uranium level around SW corner for both ARS and TRS. In ARS, the uranium trend and migrate northward from the accumulated southern section, while in TRS the uranium is truncated by moderate response and later appeared in NE corner.

The total count contour map (Figs. 6a and b) constructed in mapping out the three radioelement response depicts high similarity pattern with the thorium prevalence response maps (Figs. 4a and b) both in term of intense and low prevalence anomalous levels. It is found to range from 6.985 – 130.283 Ur in ARS and -5.893 – 30.575 Ur in TRS. Combining the three radioelement, thorium occur to be the predominant radioelement of the total count compare with uranium and potassium anomalous maps.



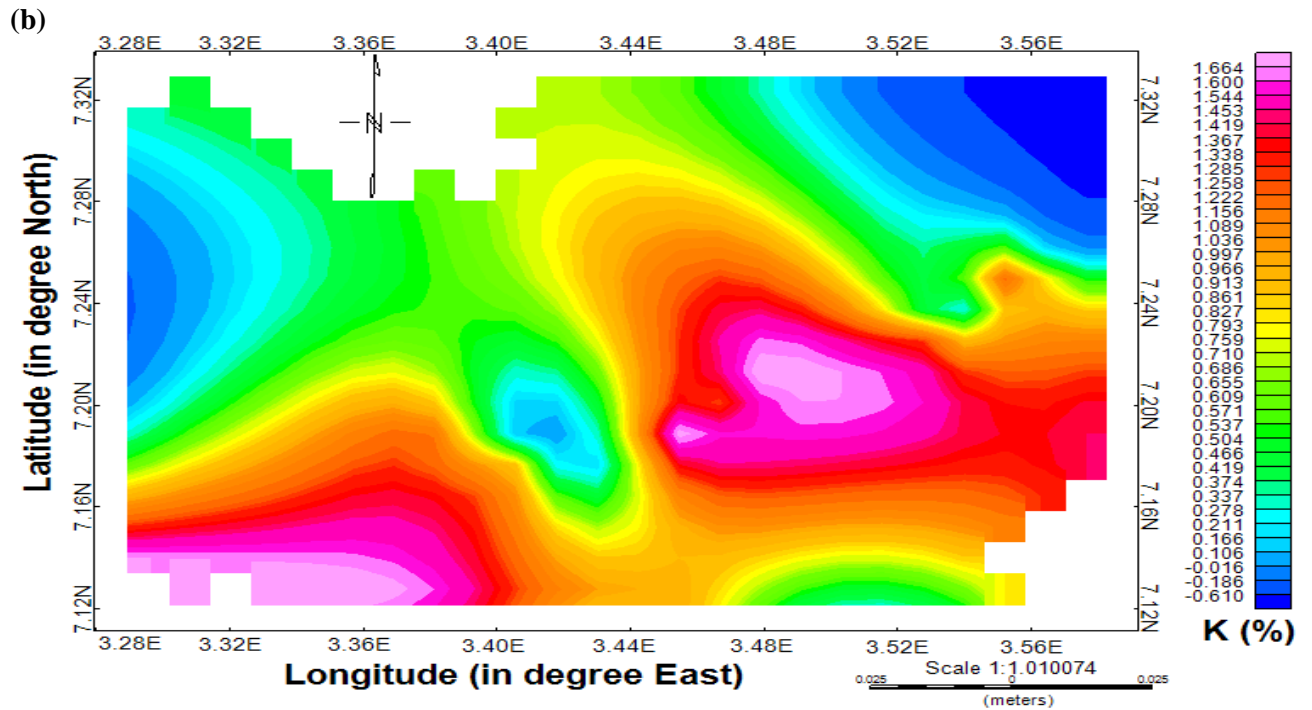
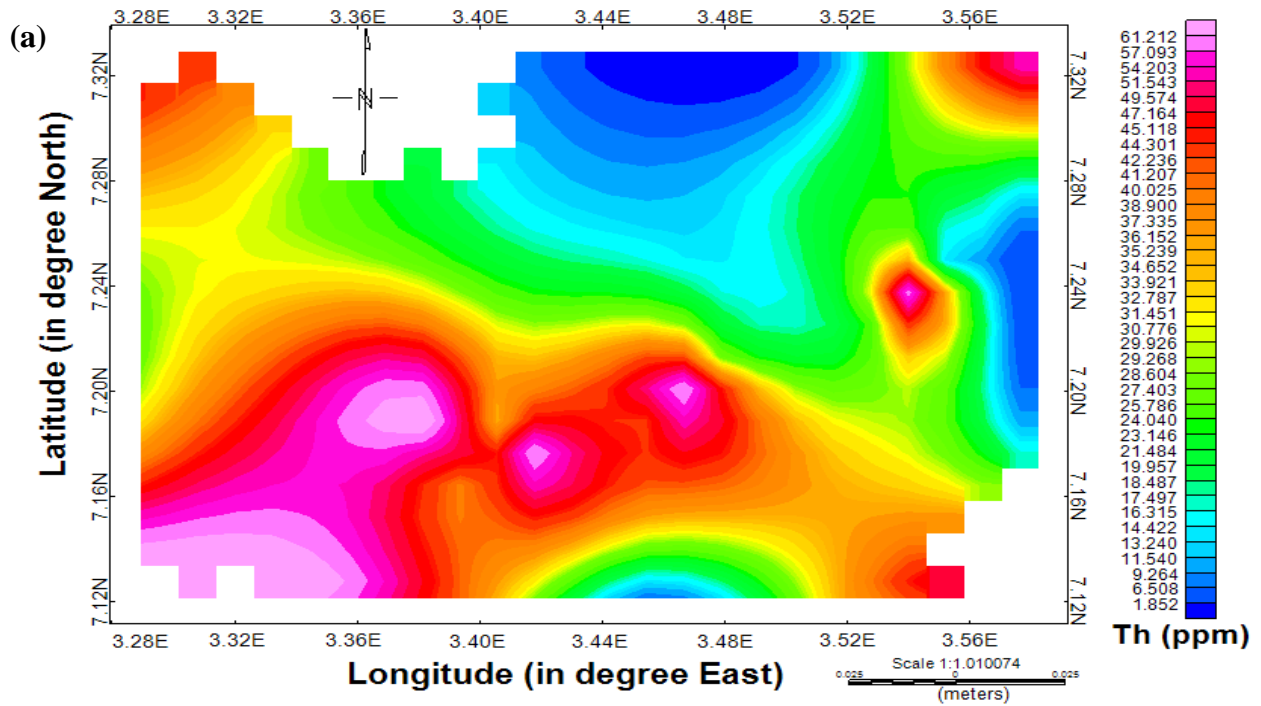


Figure 3: Contour map of potassium in (a) ARS and (b) TRS



(b)

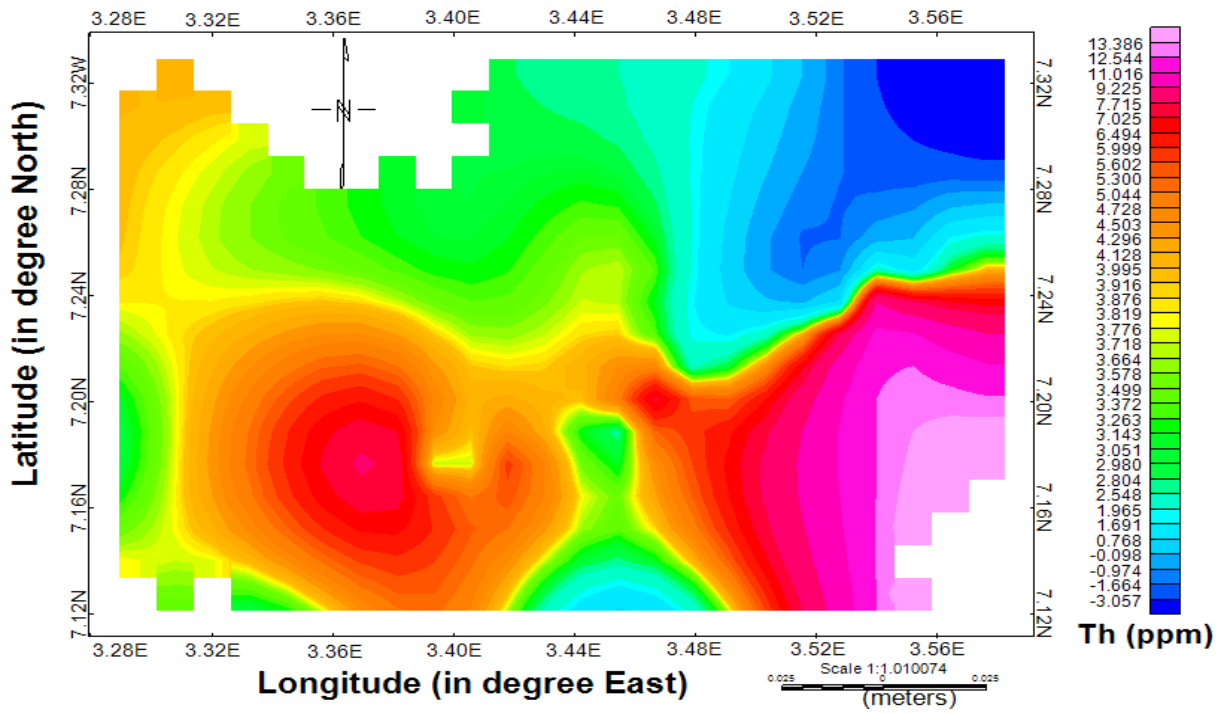
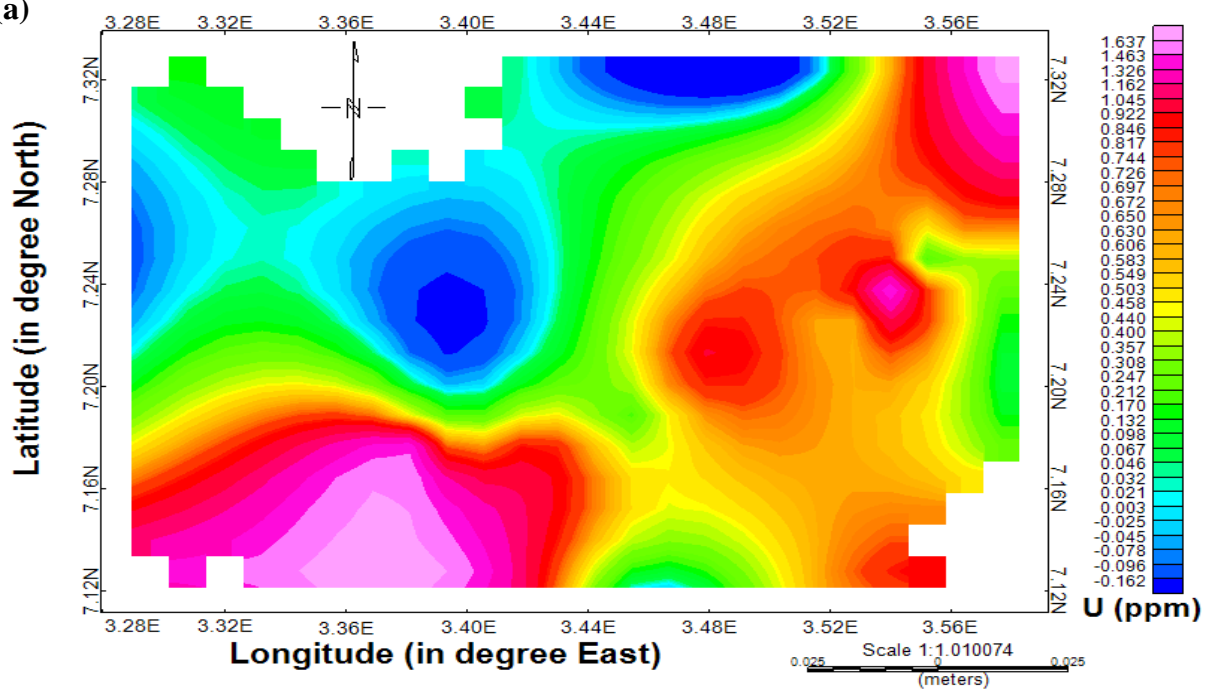


Figure 4: Contour map for thorium in (a) ARS and (b) TRS

(a)



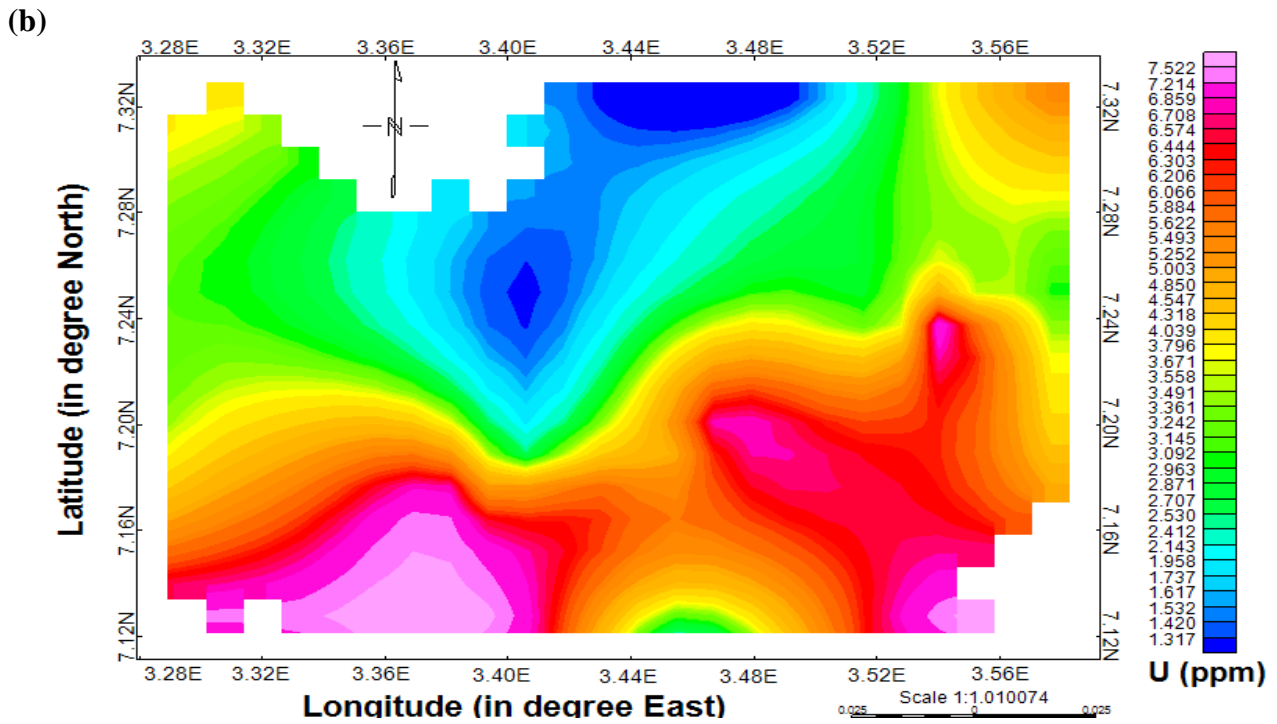
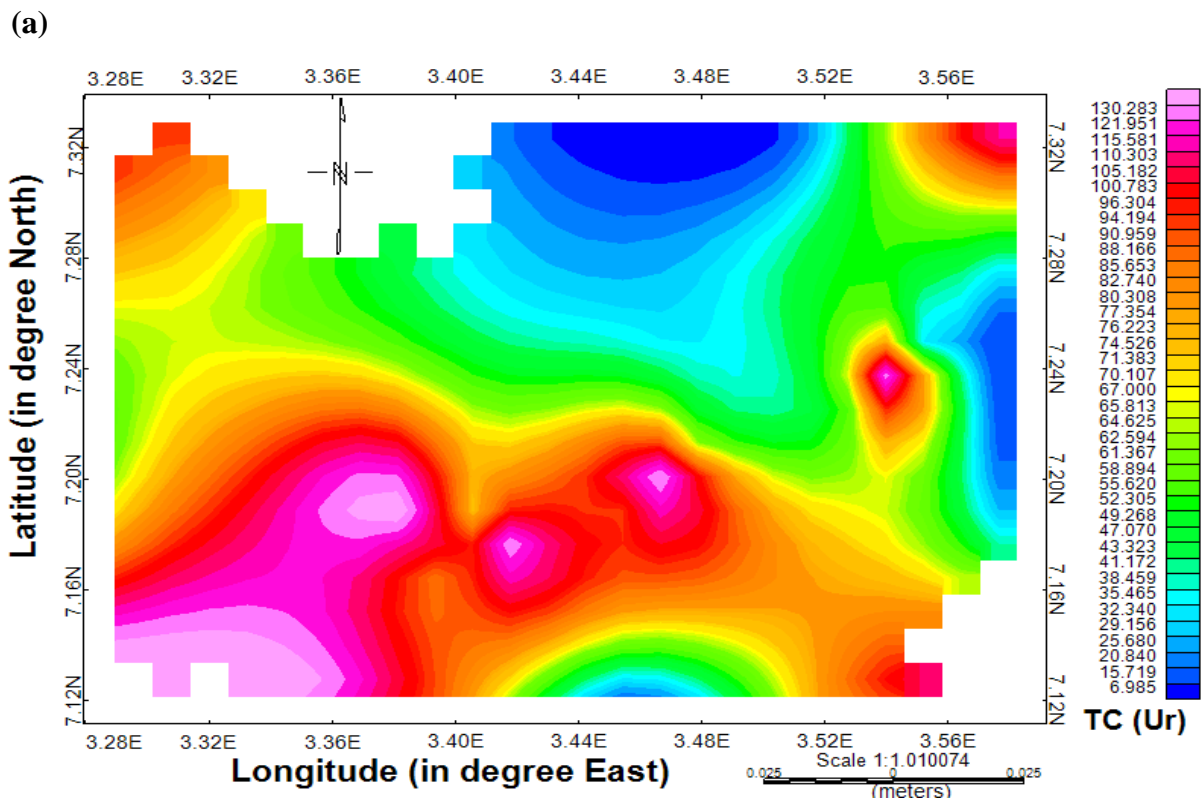


Figure 5: Contour map for uranium in (a) ARS and (b) TRS



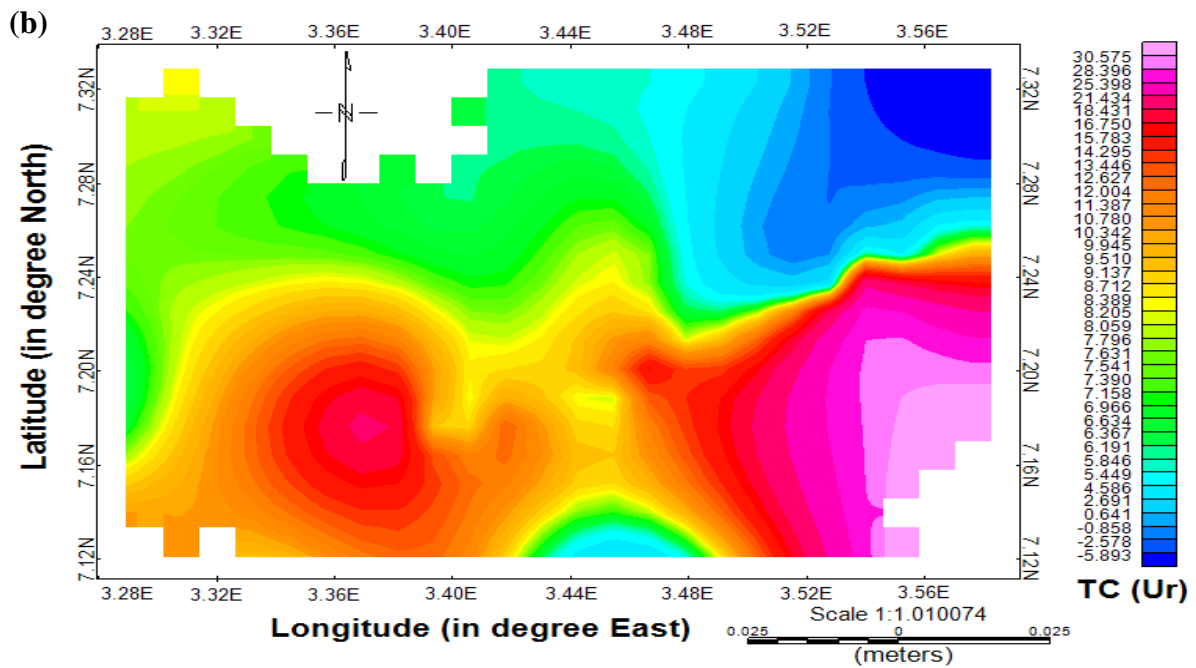
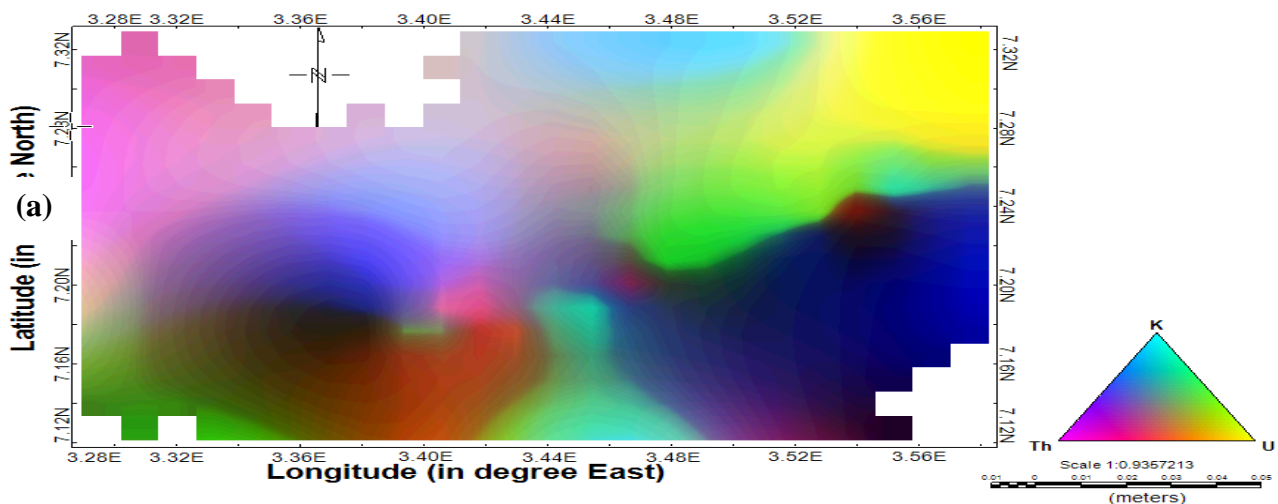


Figure 6: Contour map for total count in (a) ARS and (b) TRS

Ternary map

This is used to compliment the total cont as gives details and clear representation of the radioelement combination and their dominant region in a pictorial form. The dominant region of each radioelement is well decrbed and distinguished by varieties of colours. In this study, Figures (7a and b) depict the ternary map of ARS and TRS such that the green-magenta colour in the ternary map are used to denotes thorium abundance. The blueish-yellow describe the region of uranium deposition and reddish-cyan are indicator of potassium concentration prevalence.



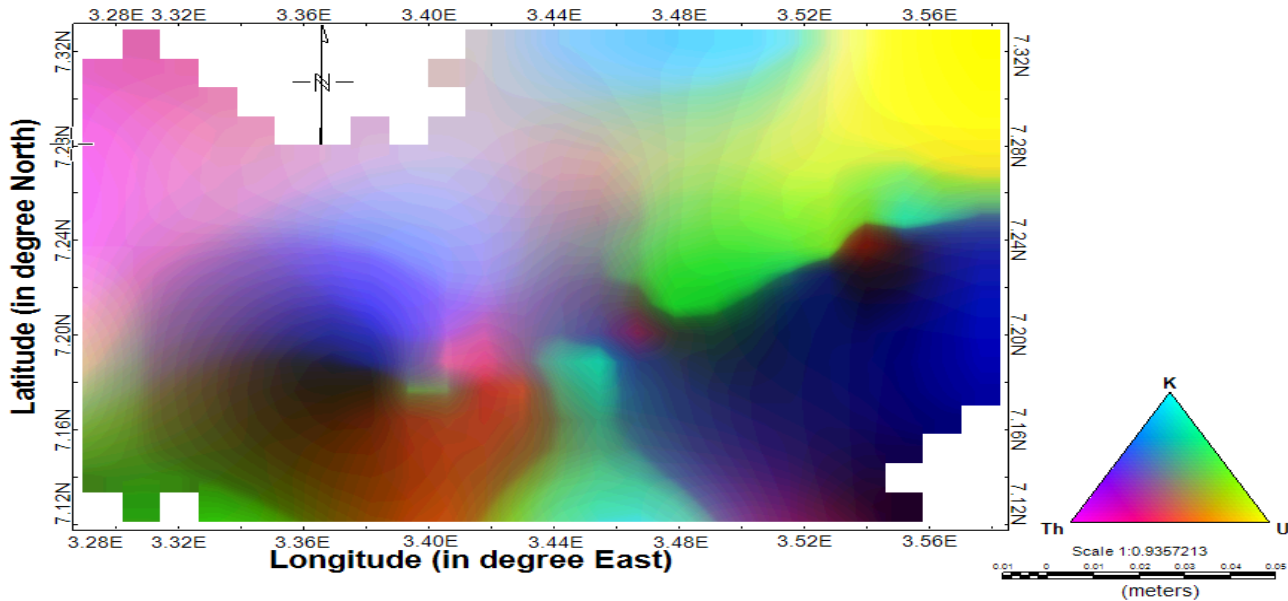


Figure 7: The ternary map of the (a) airborne and (b) ground survey

Estimated linear models

The four radiometric variables (U, Th, K and TC) were subjected to regression analysis. From this, the scatted plot was established and the linear models were generated in the order of terrestrial and airborne mode (Figures 8a- h), and vice versa for each radioelement and their respective total count as presented in equations (14 –17) and equations (18 – 21). Figure 8a and b accounted for the uranium linear model (equations 14 and 18) for ARS –TRS and TRS – ARS. Figure 8 c and d accounted for thorium ARS – TRS and TRS – ARS models in equations (15 and 19) while that of potassium ARS – TRS and TRS – ARS models (Figs. 8e and f) in equations (16 and 20). The ARS – TRS and TRS – ARS models (Figs. 8g and h) for total count was preseted in equations (17 and 21) The generated model for the radioemetric variables show that there is direct relationship between the ARS and TRS. The terrestrial survey parameters obtained can therefore be used to estimate and compute the corresponding airborne parameters, and vice versa. The coefficient correlation (r-value) obtained for the two survey are 0.81, 0.71, 0.76 and 0.71 (Table 2) for uranium, thorium, potassium and total count, respectively. The r-values showed that there is a strong link between the ARS and TRS for all the fours radiometric variables. This therefore implies that there exist no significant difference between the radiometric paramaters for the two surveys.

Computed Ground to Airborne models

$$U_A = 2.874U_G + 2.861 \tag{14}$$

$$Th_A = 4.840Th_G + 16.830 \tag{15}$$

$$K_A = 0.250K_G + 0.248 \tag{16}$$

$$TC_A = 4.816TC_G + 30.830 \tag{17}$$

Computed Airborne to Ground models

$$U_G = 0.230U_A - 0.446 \tag{18}$$

$$Th_G = 0.103Th_A + 0.291 \tag{19}$$

$$K_G = 2.294K_A + 0.375 \tag{20}$$

$$TC_G = 0.103TC_A + 1.754 \tag{21}$$

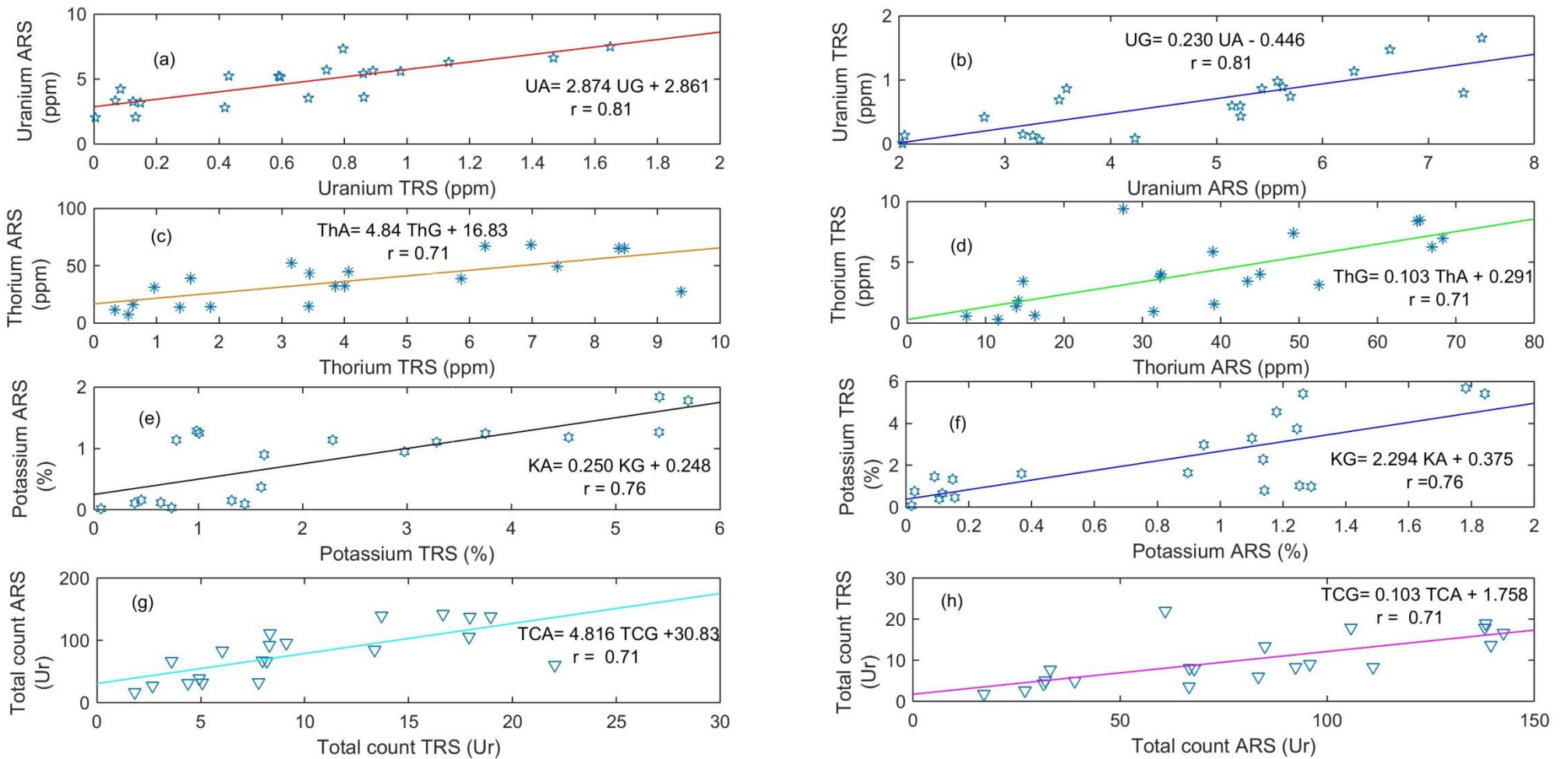


Figure 8: Scatter plot of (a) ARS – TRS for Uranium (b) TRS – ARS for Uranium (c) ARS – TRS for Thorium (d) TRS – ARS for Thorium (e) ARS – TRS for Potassium (f) TRS – ARS for Potassium (g) ARS – TRS for Total count (h) TRS – ARS for Total count

Descriptive, Normalisation and Homogeneity Analysis

The result obtained revealed uranium to range from 0.004 – 1.65 ppm and 2.03 – 7.50 ppm, with mean value of 0.63 ppm and 4.68 ppm for TRS and ARS, respectively. Thorium was accounted for in the range of 0.33 – 9.37 ppm and 7.55 – 68.35 ppm with average value 4.09 ppm and 36.80 ppm while potassium was found in the range of 0.07 – 5.69 % and 0.02 – 1.84% with mean value of 2.22% and 0.80% for TRS and ARS, respectively. The computed total count (TC) was found in the range of 1.83 – 22.05 Ur with mean value of 9.94 Ur in TRS and 17.17 – 142.51 Ur with average value of 78.69 Ur in ARS. The normalisation test showed that the mean value (X) obtained are less than the computed $X+3S$, which implies that there is little or no ambiguity in the radioelement deposit and their total count. The mineralogical interpretation of the result is an indication of presence of light minerals such as quartz, kaoline, feldspar and many others. The heavy minerals are identified if only if the $X+3S$ value is greater than the mean value.

The degree of variability of the radiometric variables are assessed with the value obtained for the coefficient of variation. This is mainly used to ascertain the extent and source of the natural environmental radiometric occurrences (Masok *et al.*, 2018). The source will be homogeneous if the CV value is less than 50% and heterogeneous for value greater than 50%. In this study, the value obtained for the coefficient of variation in TRS are 73.89, 71.22, 83.15 and 61.03 % for uranium, thorium, potassium and total count respectively. The CV result shows heterogeneous nature for all the radioelement deposits and their source. This implies that the source of the radioelement and their total count are not limited to single source. Similarly, the ARS revealed CV values of 35.27 % for uranium, 54.43 % for thorium, 75.83 % for potassium and 52.46 % for total count. Uranium showed low variability while the others reflect high variability. The two surveys showed that all the radioelements are not from single source except uranium from ARS indicating one source. The radioactive emission may be natural, lithogenic, cosmogenic and anthropogenic in nature.

The skewness result shows positive result for both TRS and ARS which implies that all the radioelectric variables analysed are skewed to the right. The kurtosis result revealed negative values for all the radiometric parameters. The kurtosis result (kurtosis < 3) implies platykurtic nature for all the radioelements.

Table 2: Descriptive, normalisation and homogeneity parameters

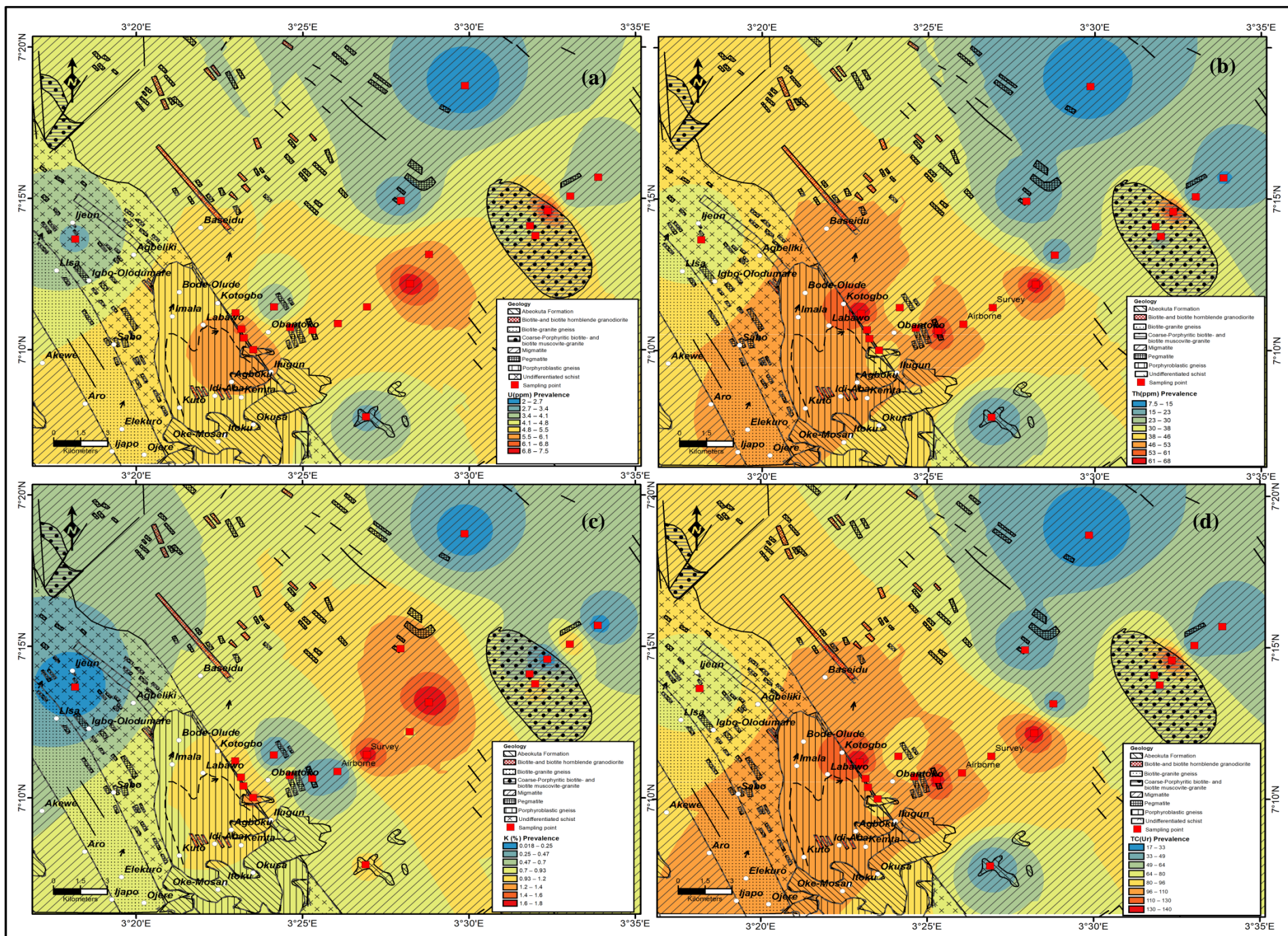
	Terrestrial Radiometric Survey (TRS)								Airborne Radiometric Survey (ARS)								r- vvalue
	Min	Max	X	S	CV	X+3S	Skew	Kurtosis	Min	Max	X	S	CV	X+3S	Skew	Kurtosis	
U (ppm)	0.004	1.65	0.63	0.46	73.89	2.04	0.49	-0.26	2.03	7.50	4.68	1.65	35.27	9.64	0.01	-0.99	0.81
Th (ppm)	0.33	9.37	4.09	2.92	71.22	12.85	0.39	-1.12	7.55	68.35	36.80	20.03	54.43	96.90	0.19	-1.16	0.71
K (%)	0.07	5.69	2.22	1.84	83.15	7.77	0.81	-0.73	0.02	1.84	0.80	0.61	75.83	2.64	0.01	-1.37	0.76
TC (Ur)	1.83	22.05	9.94	6.06	61.03	28.13	0.59	-0.87	17.17	142.51	78.69	41.29	52.46	202.54	0.18	-1.17	0.71

Geochemical superpositon

In this study, the radioelement and their total count were superimposed on the geological map to assess the degree of their anomalous responses (Figures 9 and 10) for ARS and TRS respectively.

The ARS map, accounted for low uranium concentration regions (blue colour) to range between 2.0 to 2.7 ppm and moderate region (yellow colour) ranges from 4.1 to 5.5 ppm. The region with intense uranium concentration (red colour) range from 6.8 to 7.5 ppm (Fig. 9a). Thorium (Fig. 9b) is very low in regions with blue colour ranging from 7.5 to 15 ppm, moderate in yellow regions from 38 to 46 ppm and very high in red regions from 61.0 to 68.0 ppm, while potassium (Fig. 9c) in blue covered regions has low values from 0.018 to 0.25 %, and normal in regions covered with yellow with range of 0.93 to 1.20 %, and very high in red regions ranging from 1.6 to 1.8%. The total count is very low in blue regions with magnitudes varying from 17Ur to 33Ur, moderate in regions of yellow with values ranging from 80Ur to 96Ur and very high in red regions ranging from 130 Ur - 140Ur (Fig. 9d). Thorium is found to be most prevalent when the two surveys were compared.

The superposition of TRS concentrations on the geological map revealed uranium low concentration (blue colour) to range between 0.004 to 0.13 ppm, while moderate concentration (yellow colour) and high concentration (red colour) are found in the range of 0.45 to 0.62 ppm and 1.40 to 1.60 ppm, respectively (Fig. 10a). Thorium is very low ranging from 0.33 to 0.85 ppm on regions covered with blue, moderate in regions with yellow colour ranging from 2.41 to 4.9 ppm but very high in regions with red with prevalent magnitude between 8.31 to 9.4 ppm (Fig. 10b). Potassium in the study area is very low in regions with blue ranging from 0.067 to 0.26 % very moderate in regions with yellow from 0.92 to 1.4 % but prevalently high in regions with red from 4.71 to 5.7 % (Fig. 10c). The Total counts is very low in regions with blue from 1.8 to 2.9 Ur and moderate in regions with yellow ranging from 8.11 to 11.0 Ur and very high in regions with red 19.10 to 22.0 Ur (Fig. 10d).



TASUED Journal c **Figure 9 :** Radiometric anomalous maps of (a) uranium (b) thorium, (c) potassium and (d) total count for

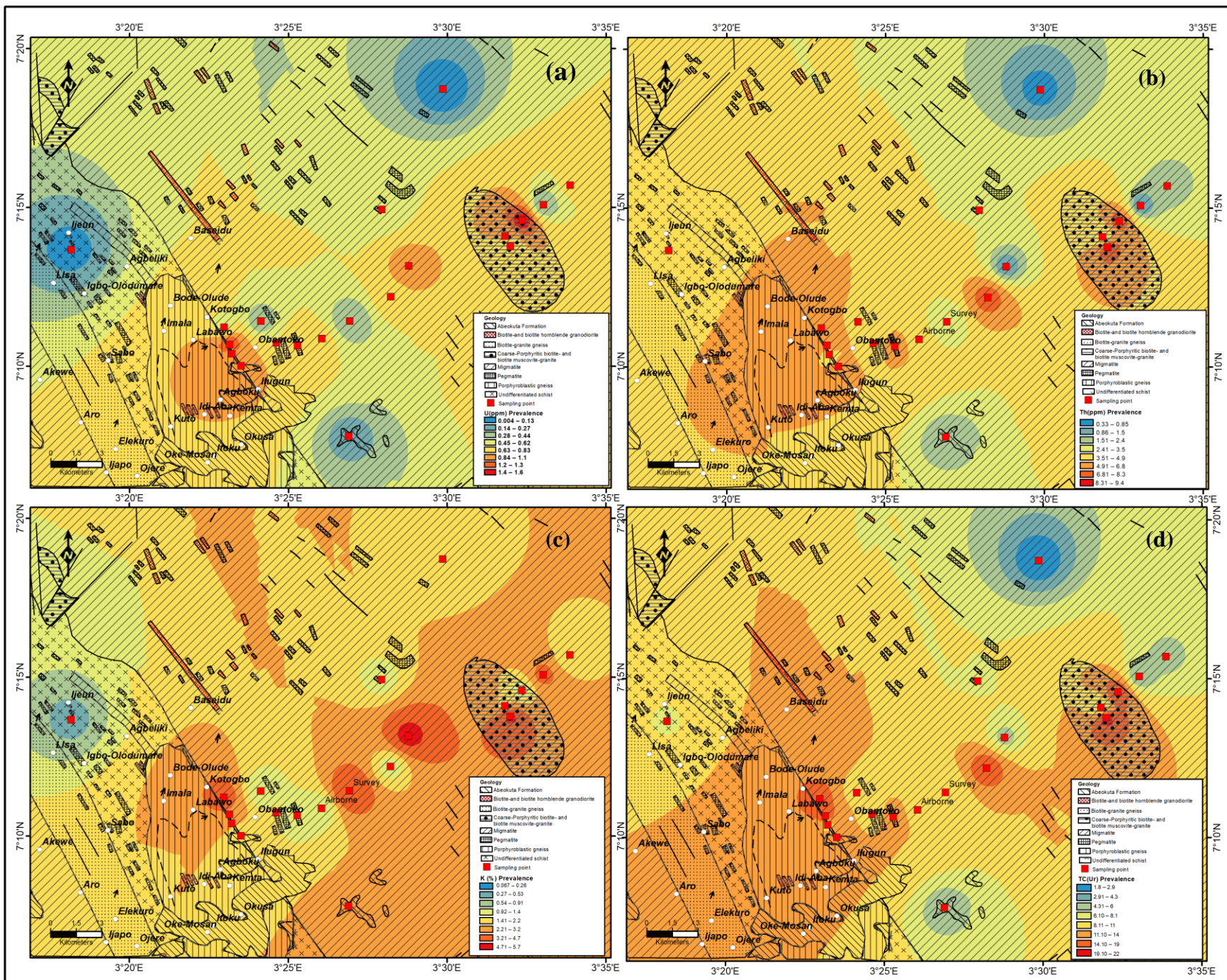


Figure 10 : Radiometric anomalous maps of (a) uranium (b) thorium (c) potassium and (d) total count for TRS

CONCLUSION

In this study, two radiometric surveys, TRS and ARS were employed to investigate the radioelement response to the bedrock composition and the following deduction are made:

- (i) Based on the regression model developed, if components of one of the surveyed radiometric parameters are known, the others can be deduced.
- (ii) The normalisation test ($X+3S$) can be used to delineate the presence of light or heavy minerals. In this study light minerals were identified from the radiometric response.
- (iii) The study area, being a weathered zone, revealed heterogeneous source of radiometric deposits due to geomorphic processes such as intrusion, faults and fractures.
- (iv) Thorium is found to be the most prevalent across the study area compared to uranium and potassium.
- (v) Although different values were obtained for each radiometric component, but surprisingly, both ARS and TRS results revealed similar radiometric anomalous responses.
- (vi) The statistical analysis indicates that there exist no significant difference between ARS and TRS.

REFERENCES

- Abbadly, A.G.E and Al-Ghamdi, A.H (2018). Heat production rate from radioactive elements of granite rocks in north and southeastern Arabian shield Kingdom of Saudi Arabia. *J Radiat Res Appl Sci* 11:281–290
- Abuelnaga, H.S., and Al-Garni, M.A. (2015). Airborne gamma-ray spectrometric and magnetic studies of Wadi Um Geheig-Wadi Abu Eligam area, Central Eastern Desert, Egypt. *Arabian Journal of Geosciences*, 8, pp. 8811–8833, DOI: 10.1007/s12517-015-1820-9.
- Adagunodo, T.A., Bayowa, O.G., Ojoawo, I.A., Usikalu, M.R and Omeje, M (2019). Radiogenic Heat Model in the southern axis of Ogbomoso, SW Nigeria. In: International conference on science and sustainable development. *Journal of Physics: Conference Series* 1299:012074
- Ashwal LD, Morgan P, Kelly SA, Preicival GA (1987). Heat production in an Archean crustal profile and implications for heat flow and mobilization of heat producing elements. *Lett Earth Planet Sci* 85:439–450
- Badmus, B.S. and Olatinsu, O.B., (2010). Aquifer characteristics and groundwater recharge pattern in typical basement complex, south western Nigeria. *Afr. J. Environ. Sci. Technol.* 4 (6), 328–342.
- Carvalho, C., Anjos, R., Veiga, R. and Macario, K (2011). Application of radiometric analysis in the study of provenance and transport processes of Brazilian coastal sediments. *J. Environ. Radioact.* 102 (2), 185–192
- Eisenbud, M and Gesell, T (1997). *Environmental Radioactivity*. (Fourth Edition) Elsevier ISBN: 978-0-12-235154-9
- Faure, G. (1986). *Principles of Isotope Geology*, second ed., John Wiley & Sons, 471864129.
- Fu, H, Jian, X, Liang, H, Zhang, W, Shen, X, and Wang, L. (2022). Tectonic and climatic forcing of chemical weathering intensity in the northeastern Tibetan Plateau since the middle Miocene. *Catena* 208 105785 <https://doi.org/10.1016/j.catena.2021.105785>

- Grasty, R.L., Holman, P.B and Blanchard, Y.B (1991). Transportable calibration pads for ground and airborne gamma-ray spectrometers. Geological Survey of Canada, Internal Report (IR- 90), p 23
- Haneklaus, N (2021). Unconventional uranium resources from phosphates. *Encycl Nucl Energy* 286–291. <https://doi.org/10.1016/B978-0-12-819725-7.00152-5>
- Hasterok ,D., Gard, M. and Webb, J (2018). On the radiogenic heat production of metamorphic, igneous, and sedimentary rocks. *Geosci Front* 9:1777–1794
- International Atomic Energy Agency, IAEA (2003) Guidelines for radioelement mapping using gamma ray spectrometry data. IAEATECDOC-1363, Vienna, Austri,14 p.
- Karim, Z , Qureshi, B.A.L and Mumtaz, M. (2015) Geochemical baseline determination and pollution assessment of heavy metals in urban soils of Karachi, Pakistan, *Ecol. Indic.* 48 358–364 .
- Malczewski, D., Taper, L and Dorda, J (2004) Assessment of natural and anthropogenic radioactivity levels in rocks and soils in the environs of swieradowzdroj in sudetes, Poland by in situ gamma-ray spectrometry. *J Environ Radioact* 73:233–245
- Masok, F.B. Masiteng, P.L. Mavunda, R.D. Maleka, P.P. and Winkler, H. (2018). Measurement of radioactivity concentration in soil samples around phosphate rock storage facility in Richards Bay, South Africa. *Journal of Radiation Research and Applied Sciences*, 11(1), pp. 29–36. DOI: 10.1016/j.jrras.2017.10.006.
- McCay, A.T, Harley, T.L, Younger, P.L., Sanderson, D.C and Cresswell, A.J (2014) Gamma-ray spectrometry in geothermal exploration: state of the art techniques. *Energies* 7(8):4757–4780
- Menager, M.T., Heath, M.J., Ivanovich, M., Montjotin, C., Barillon, C.R., Camp, J. and Hasler, S.E. (1993). Migration of uranium from uranium-mineralised fractures into the rock matrix in granite: implications for radionuclide transport around a radioactive waste repository, in: Fourth Inter. Conference of Chemistry and Migration Behaviour of Actinides and Fission Products in the Geosphere (Migration 1993), Charleston, USA, 12E17. *Radiochimica Acta* 66/67 ,pp. 47-83.
- Murugesan, S., Mullainathan, S., Ramasamy V, Meenakshisundaram V (2011) Radioactivity and radiation hazard assessment of Cauvery River, Tamilnadu, India. *Iran J Radiat Res*, 8(4): 211 – 222.
- NCRP, (1984). National council on radiation protection and measurements. In: Control of Air Emissions of Radionuclides, NCRP Statement No. 6 (National Council on Radiation Protection and Measurements, Bethesda, Maryland), 183.
- Nigeria Geological Surveys Agency, (NGSA) (2019). Lineaments Map of Nigeria Scale 1: 2,000,000, Second edition. Published by Authority of Federal Republic of Nigeria
- Olorunsola, K and Aigbogun, C (2017). Correlation and mapping of geothermal and radioactive heat production from the Anambra Basin, Nigeria. *Afr J Environ Sci Technol* 11(10):517– 531
- Omatsola, M.E. and Adegoke, O.S.,(1981). Tectonic evolution and Cretaceous stratigraphy of the Dahomey basin. *J. Min. Geol.* 5 (2), 78–83.
- Ogunsanwo, F.O., Olowofela, J.A., Okeyode, I.C., Idowu, O.A and Olurin, O.T. (2019). Aeoradiospectrometry in the spatial formation characterization of Ogun State, south-western, Nigeria. *Scientific African* 6, 204.

- Ogunsanwo, F. O., Adepitan, J. O., Ayanda, J. D., Giwa, K. W., Falayi, E. O. and Adejimi, A. I. (2021). Radiogenic heat production in crustal quarry rocks of Ogun State, south-western, Nigeria, *Environmental Earth Sciences* , 80:282 <https://doi.org/10.1007/s12665-021-09578-7>
- Peng, J., Yu, J., Zheng, D., Wang, W., Ma, Y., Wang, Y., Li, C., Li, Y. and Wang, Y., (2019). Neogene expansion of the Qilian Shan, north Tibet: Implications for the dynamic evolution of the Tibetan Plateau. *Tectonics* 38 (3), 1018–1032. <https://doi.org/10.1029/2018TC005258> .
- Polito, P., Kyser, T., Alexandre, P., Hiatt, E and Stanley, C (2011). Advances in understanding the Kombolgie Subgroup and unconformity-related uranium deposits in the Alligator Rivers Uranium Field and how to explore for them using lithogeochemical principles. *Aust. J. Earth Sci.* 58, 453–474.
- Rahaman, M.A (1976). Review of the basement geology of southwestern Nigeria. In C.A Kogbe (Ed), *Geology of Nigeria*, Elizabethan Publ. Co., Lagos, pp 41-58.
- Ramadass, G., SubhashBabu, A. and Udaya, L.G., (2015). Structural analysis of airborne radiometric data for identification of Kimberlites in parts of Eastern Dharwar Craton. *Int. J. Sci. Res.* 4 (4), 2379–2380.
- Singh, A.K and Vallinayagam, G (2004) Geochemistry and petrogenesis of anorogenic basic volcanic-plutonic rocks of the Kundal area of Malani Igneous Suite, Western Rajasthan. *India Proc Ind Acad Sci (Earth Planetary Science)* 113:667–681
- Steiner, G., Geissler, B. and Haneklaus, N (2020) Making uranium recovery from phosphates great again? *Environ Sci Technol* 54:1287–1289. <https://doi.org/10.1021/acs.est.9b07859>
- Sun Y, Amelung W, Wu B et al (2022) Fertilizer P-derived uranium continues to accumulate at Rothamsted long-term experiments. *Sci Total Environ* 820:153118. <https://doi.org/10.1016/j.scitotenv.2022.153118>
- Talabi, A.O. (2015). Weathering of meta-igneous rocks in parts of the basement terrain of south-western, Nigeria: implications on groundwater occurrence. *International Journal of Scientific and Research Publications*, 5, 1 – 17. <http://www.ijsrp.org/research-paper-0415.php?rp=P403886>
- Tzortzis, M. And Tsertos, H. (2004) Determination of thorium, uranium and potassium elemental concentrations in surface soils in Cyprus, *J. Environ. Radioact.* 77325-338
- UNSCEAR, (2000). United Nation Scientific Committee on the Effect of Atomic Radiation. Sources and Effects of Ionizing Radiation. Report to General Assembly, with Scientific Annexes. United Nations, New York.
- Veikkolainen, T and Kukkonen, I.T (2019) Highly varying radiogenic heat production in Finland, Fennoscandian Shield. *Tectonophysics* 750:93–116
- Wilton, D.H.C. and Cunningham-Dunlop, I., (2006). The exploration activities of Aurora- Energy Inc. on the CMB uranium property, Labrador, Canada, during the period of June 2005 to December 2005. In: Prepared for Aurora-Energy Inc, p. 137. NI 43–101F1 Technical Report.
- Ye, Y., Al-Khaleedi, N and Barker, L et al (2019). Uranium resources in China's phosphate rocks – identifying low-hanging fruits. *IOP Conf Ser: Earth Environ. Sci.* 227:052033. <https://doi.org/10.1088/1755-1315/227/5/052033>

Yu, X., Guo, Z., Chen, Y., Cheng, X., Du, W and Wang, Z. (2021). Recognition and application of offlap in endorheic basins: new insights into plateau growth. *Int. Geol. Rev.* 1–16
<https://doi.org/10.1080/00206814.2021.1894611>